Estimating mass discharge from dense nonaqueous phase liquid source zones using upscaled mass transfer coefficients: An evaluation using multiphase numerical simulations

John A. Christ,[1] C. Andrew Ramsburg,[2] Kurt D. Pennell,[3,4] and Linda M. Abriola[2]

[1] Difficulties associated with identifying the dense nonaqueous phase liquid (DNAPL) source zone architecture at the field scale, combined with the computational costs of field-scale DNAPL dissolution simulations, have motivated the development of a number of simplified models that rely upon upscaled (i.e., domain-averaged) mass transfer coefficients to approximate field-scale dissolution processes. While conceptually attractive, these upscaled models have yet to be fully evaluated for prediction of mass recovery from a range of nonuniform, three-dimensional DNAPL source zones. This study compares upscaled model predictions of flux-weighted downstream concentrations and source longevity to predictions derived from three-dimensional multiphase numerical simulation of tetrachloroethene (PCE)-NAPL dissolution for realizations of a statistically homogeneous, nonuniform aquifer. Although the functional forms of the upscaled models are generally shown to be mathematically equivalent, upscaled model flux-weighted concentration predictions varied by over one order of magnitude, with variations attributed to the dependence of the upscaled model parameters on the specific source zone scenario used for model calibration. Replacement of upscaled model calibration parameters with source zone parameters that can be obtained from site characterization information (specifically, the initial flux-weighted concentration and source zone ganglia-to-pool (GTP) mass ratio) reduced the root-mean-square error between upscaled and numerical model predictions by approximately 80%. Application of this modified model to a range of source zone scenarios ($0.4 < GTP < \infty$) demonstrates the efficacy of the model for use as a screening tool to relate DNAPL mass removal and flux-weighted concentrations when mass removal is less than 80%.

1. Introduction

[2] The presence of dense nonaqueous phase liquid (DNAPL) at a site is a critical factor in the design and efficacy of any site remediation strategy [*Mackay and Cherry*, 1989]. When released into an aquifer, a DNAPL can become entrapped as discontinuous ganglia [*U.S. Environmental Protection Agency* (*USEPA*), 1990; *Mercer and Cohen*, 1990] and accumulate in higher saturation pools at textural interfaces within the medium [*Kueper et al.*, 1993], serving as a long-term source of dissolved phase contamination. The region of a contaminated aquifer containing DNAPL pools and ganglia is frequently referred to as a source zone [*National Research Council* (*NRC*), 2005]. Recently, research has focused on quantifying the potential benefits of DNAPL source zone mass removal, including reductions in down-gradient contaminant concentrations, mass flux, and DNAPL source longevity [*Berglund*, 1997; *Dekker and Abriola*, 2000b; *Sale and McWhorter*, 2001; *Rao et al.*, 2001; *Rao and Jawitz*, 2003; *USEPA*, 2003; *Lemke et al.*, 2004b; *Parker and Park*, 2004; *Soga et al.*, 2004; *Wood et al.*, 2005; *Jawitz et al.*, 2005; *Fure et al.*, 2006]. A number of researchers have developed screening models that relate reductions in down-gradient contaminant concentration and source longevity to the level of mass removal [*Dekker*, 1996; *Parker and Park*, 2004; *Zhu and Sykes*, 2004; *Falta et al.*, 2005a; *Park and Parker*, 2005; *Jawitz et al.*, 2005; *Fure et al.*, 2006]. These models are typically simplified parametric or analytical expressions of reduced dimensionality. The development of these models has been motivated by difficulties associated with applying more comprehensive modeling tools, including description of DNAPL source zone architecture at the field scale and computational costs of field-scale dissolution simulations. The general utility of these screening models, however, is unclear given that they cannot be used in a

[1]Department of Civil and Environmental Engineering, U.S. Air Force Academy, Colorado Springs, Colorado, USA.
[2]Department of Civil and Environmental Engineering, Tufts University, Medford, Massachusetts, USA.
[3]School of Civil and Environmental Engineering, Georgia Institute of Technology, Atlanta, Georgia, USA.
[4]Also at Department of Neurology, Emory University School of Medicine, Atlanta, Georgia, USA.

Report Documentation Page

1. REPORT DATE **2006**	2. REPORT TYPE	3. DATES COVERED **00-00-2006 to 00-00-2006**

4. TITLE AND SUBTITLE	5a. CONTRACT NUMBER
Estimating Mass Discharge From Dense Nonaqueous Phase Liquid Source Zones Using Upscaled Mass Transfer Coefficients: An Evaluation Using Multiphase Numerical Simulations	5b. GRANT NUMBER
	5c. PROGRAM ELEMENT NUMBER
6. AUTHOR(S)	5d. PROJECT NUMBER
	5e. TASK NUMBER
	5f. WORK UNIT NUMBER

7. PERFORMING ORGANIZATION NAME(S) AND ADDRESS(ES) **U.S. Air Force Academy,Department of Civil and Environmental Engineering,Colorado Springs,CO**	8. PERFORMING ORGANIZATION REPORT NUMBER

9. SPONSORING/MONITORING AGENCY NAME(S) AND ADDRESS(ES)	10. SPONSOR/MONITOR'S ACRONYM(S)
	11. SPONSOR/MONITOR'S REPORT NUMBER(S)

12. DISTRIBUTION/AVAILABILITY STATEMENT
Approved for public release; distribution unlimited

13. SUPPLEMENTARY NOTES

14. ABSTRACT

15. SUBJECT TERMS

16. SECURITY CLASSIFICATION OF:			17. LIMITATION OF ABSTRACT	18. NUMBER OF PAGES	19a. NAME OF RESPONSIBLE PERSON
a. REPORT **unclassified**	b. ABSTRACT **unclassified**	c. THIS PAGE **unclassified**	**Same as Report (SAR)**	**13**	

predictive sense due to the need to calibrate model parameters to specific site conditions.

[3] Simplified screening models may be divided into two categories: (1) stochastic-advective models, which relate source zone remediation performance to joint spatial variability of both groundwater flow and NAPL content [*Berglund*, 1997; *Jawitz et al.*, 2003, 2005; *Enfield et al.*, 2005; *Wood et al.*, 2005; *Fure et al.*, 2006], and (2) upscaled models (sometimes referred to as macroscopic, effective, or field scale), which incorporate the effects of spatial variations in DNAPL saturations and flow bypassing on source zone mass discharge through the use of an upscaled (i.e., domain-averaged) mass transfer coefficient [*Parker and Park*, 2004; *Zhu and Sykes*, 2004; *Falta et al.*, 2005a; *Park and Parker*, 2005; *Basu et al.*, 2006]. Stochastic-advective models have been used to approximate the response in contaminant mass flux due to DNAPL source depletion using trajectory-averaged model parameters [*Wood et al.*, 2005; *Fure et al.*, 2006]. These trajectory-averaged model parameters are flow field specific and are typically obtained by interrogating the swept volume with a tracer or suite of tracers [*Jawitz et al.*, 2003; *Enfield et al.*, 2005]. In contrast, upscaled modeling methods have been employed to quantify the relationship between DNAPL mass and source strength [*Falta et al.*, 2005a, 2005b; *Basu et al.*, 2006]. Application of these upscaled models does not require imposition of the remedial flow field and may thus prove better suited for incorporating the information gained during a typical site characterization effort into a remedial design. The present work is restricted to consideration of upscaled modeling methods [*Parker and Park*, 2004; *Zhu and Sykes*, 2004; *Falta et al.*, 2005a; *Park and Parker*, 2005].

[4] Upscaled models typically assume that the flow field is steady and dissolution mass transfer can be approximated by a linearized Fick's law expression incorporating an upscaled (i.e., domain-averaged) mass transfer coefficient. Upscaled mass transfer coefficients have been estimated using explicit descriptions of pore networks and NAPL saturation distribution [*Jia et al.*, 1999; *Held and Celia*, 2001; *Sale and McWhorter*, 2001], or by fitting solutions of a simplified one-dimensional component mass balance equation to experimental [*Saba and Illangasekare*, 2000; *Schaerlaekens and Feyen*, 2004] or numerically generated results [*Dekker*, 1996; *Parker and Park*, 2004; *Zhu and Sykes*, 2004; *Park and Parker*, 2005]. In the latter cases, the upscaled mass transfer coefficient has generally been correlated with several simulation parameters including groundwater velocity, mean hydraulic conductivity, and the extent of mass removal using best fit correlation parameters. These upscaled mass transfer correlations are similar in form to correlations that have been derived in other studies to describe local-scale dissolution under a variety of conditions, including dissolution of residual NAPL ganglia [e.g., *Miller et al.*, 1990; *Geller and Hunt*, 1993; *Powers et al.*, 1994; *Imhoff et al.*, 1994], dissolution from high initial saturation ganglia regions [e.g., *Nambi and Powers*, 2000, 2003], interphase mass exchange from DNAPL pools [e.g., *Kim and Chrysikopoulos*, 1999; *Chrysikopoulos and Kim*, 2000], and dissolution from a source emplaced in the field [*Frind et al.*, 1999; *Broholm et al.*, 1999, 2005; *Rivett and Feenstra*, 2004]. Unlike the local-scale mass transfer correlations, which have demon-

strated applicability for a range of porous media, flow and entrapment conditions [e.g., *Powers et al.*, 1994; *Imhoff et al.*, 1994], existing upscaled mass transfer correlations tend to be site specific, valid only for sites with conditions (i.e., source zone architectures) consistent with those used to parameterize the upscaled mass transfer correlation [*Parker and Park*, 2004].

[5] Despite their simplicity and conceptual attractiveness, the utility of the upscaled model as an alternative to computationally intensive numerical simulations is limited unless upscaled mass transfer coefficient correlations can be developed that apply to a broad range of sites. The objectives of this work are (1) to demonstrate the predictive limitations of existing upscaled mass transfer models, through comparison with three-dimensional numerical simulations of dissolution from representative DNAPL source zones, (2) to develop an improved formulation that facilitates independent estimation of model parameters over a wide range of source zone scenarios, and (3) to evaluate the predictive capability of this improved upscaled mass transfer model. The source zone scenario selected for these evaluations was based on the Bachman Road site, which was extensively characterized as part of a pilot-scale surfactant enhanced aquifer remediation (SEAR) demonstration [*Abriola et al.*, 2005; *Ramsburg et al.*, 2005]. This site is representative of many small-scale DNAPL source zones located throughout the United States [*Abriola et al.*, 2005].

2. Methodology

[6] The objectives of this work require the use of both numerical and analytical methods to model mass discharge from DNAPL source zones. Comprehensive reviews of compositional multiphase numerical models can be found in the literature [*Abriola*, 1989; *Miller et al.*, 1998; *Adeel et al.*, 2001]. Likewise, analytical models describing contaminant fate and transport are discussed in most groundwater textbooks [e.g., *Bear*, 1979; *Fetter*, 1993]. Therefore this section includes only a brief review of the equations governing multiphase, multicomponent flow. Simplifying assumptions, equation solution techniques, and site conditions employed in the simulations are presented for both the numerical and analytical models.

2.1. Governing Equations

[7] Simulation of a DNAPL spill and subsequent contaminant mass discharge in the saturated zone requires the solution of both phase and component mass balance equations. Phase mass balance equations describe bulk fluid phase flow using a modified form of Darcy's equation and constitutive relationships for saturation, relative permeability, and capillary pressure [see *Abriola*, 1989]. Within each bulk fluid phase (aqueous, $\alpha = a$; organic, $\alpha = n$), the spatial-temporal distribution of component i is computed using a component mass balance equation written in terms of the mass concentration of component i in the α phase (C_i^α):

$$\phi \frac{\partial}{\partial t}\left(s_\alpha C_i^\alpha\right) + \phi \nabla \cdot s_\alpha \left(C_i^\alpha V^\alpha - \boldsymbol{D_\alpha^i} \cdot \nabla C_i^\alpha\right) = \sum_\beta E_{\alpha\beta_i} \quad (1)$$

ϕ is the matrix porosity, s_α is the α phase saturation, $\boldsymbol{D_\alpha^i}$ is the three-dimensional hydrodynamic dispersion tensor for

component i in phase α [*Bear*, 1972], V^α is the α phase pore velocity computed using a modified form of Darcy's law [*Abriola*, 1989], and $E_{\alpha\beta i}$ is the interphase mass exchange of component i from the β to the α phase [*Weber and DiGiano*, 1996]:

$$E_{\alpha\beta i} = \kappa_{\alpha\beta i}\left(C_i^{\alpha\,eq} - C_i^\alpha\right) \qquad (2)$$

where $C_i^{\alpha eq}$ is the equilibrium solubility of component i in the α phase, and $\kappa_{\alpha\beta i}$ is a lumped mass transfer coefficient, which quantifies the rate of mass transfer of component i from the β to the α phase. This lumped coefficient ($\kappa_{\alpha\beta i}$) is generally represented as a correlation between a Sherwood number ($N_{Sh} = \kappa_{\alpha\beta i}d_{50}^2/D_m$), normalized DNAPL saturation ($s_n/s_n^{t=0}$), Reynolds number ($N_{Re} = V^a\rho_a d_{50}/\mu_a$), and Schmidt number ($N_{sc} = \mu_a/\rho_a D_m$), where d_{50} is the mean grain diameter, and D_m is the aqueous phase molecular diffusion coefficient [e.g., *Miller et al.*, 1990; *Imhoff et al.*, 1994; *Powers et al.*, 1994]. Incorporation of the normalized saturation into the lumped mass transfer coefficient accounts for the transient nature of the lumped mass transfer coefficient resulting from reductions in interfacial area as the DNAPL ganglia dissolve.

[8] Solution of the phase and component mass balance equations permits the quantification of several commonly employed source zone management metrics which may be used to assess the performance of the upscaled model: (1) flux-weighted concentration at a down-gradient boundary or point of compliance, (2) contaminant mass flux across a down-gradient boundary, and (3) source longevity. These metrics have been used extensively to quantify the benefits of partial mass removal from DNAPL source zones [*Dekker and Abriola*, 2000b; *Einarson and Mackay*, 2001; *Sale and McWhorter*, 2001; *McWhorter and Sale*, 2003; *Rao et al.*, 2001; *Saenton et al.*, 2002; *Rao and Jawitz*, 2003; *Lemke et al.*, 2004b; *Soga et al.*, 2004; *Broholm et al.*, 2005; *Jawitz et al.*, 2005; *Fure et al.*, 2006; *Basu et al.*, 2006], and have recently been proposed as an alternative to more traditional remediation metrics, such as maximum contaminant concentration [*Stroo et al.*, 2003; *USEPA*, 2003; *NRC*, 2005].

2.2. Numerical Simulations

[9] Source zone distributions have generally been characterized using domain-averaged NAPL saturations, stochastic-advective trajectory averaged NAPL saturations [e.g., *Jawitz et al.*, 2005], or ganglia-to-pool (GTP) mass ratios [*Lemke et al.*, 2004b; *Christ et al.*, 2003; *Lemke and Abriola*, 2006]. While each of these metrics has utility, the GTP mass ratio is selected for analysis herein due to its potential to link mass discharge strength to source zone architecture in nonuniform macroscopic 3-D domains. Applicability to nonuniform domains is a clear limitation of existing upscaled mass transfer models [e.g., *Falta et al.*, 2005a; *Wood et al.*, 2005; *Basu et al.*, 2006].

[10] GTP mass ratios quantify the distribution of DNAPL between ganglia and pool regions according to

$$\mathrm{GTP} = \frac{\sum \rho_n s_n \phi \Delta x \Delta y \Delta z \forall s_n < s_{nr}^{\max}}{\sum \rho_n s_n \phi \Delta x \Delta y \Delta z \forall s_n \geq s_{nr}^{\max}} = \frac{\sum s_n \forall s_n < s_{nr}^{\max}}{\sum s_n \forall s_n \geq s_{nr}^{\max}} \qquad (3)$$

Here pooled regions are defined as source zone regions (numerical grid blocks) with a saturation greater than the

maximum residual organic saturation ($s_{nr}^{\max}$), which corresponds to the aqueous phase saturation reached upon complete imbibition from the residual water saturation point on the drainage curve [*Parker and Lenhard*, 1987], and ganglia regions are defined as regions with DNAPL saturations at or below $s_{nr}^{\max}$. In the initial stages of source evolution, mass discharge is controlled by the dissolution of high surface area ganglia. During this period, GTP decreases exponentially with time (linearly with the fraction of mass removed) (results not shown). At later time, the persistence of DNAPL pools causes the source zone to transition from ganglia-dominated to pool-dominated. Thus initial source zone architecture may have significant influence on mass discharge [*Lemke et al.*, 2004b; *Lemke and Abriola*, 2006].

[11] Previous research on upscaled modeling methods has focused on the simulation of DNAPL source zones which are characterized in this work as end-members on a continuum of potential DNAPL source zone distributions. At one end of the continuum of source zone distributions lies the hypothetical source zone with a uniform DNAPL distribution at residual saturation (e.g., $s_n = 0.01$, GTP $= \infty$, used by *Zhu and Sykes* [2004] to simulate mass discharge). Near the opposite end of the continuum lies an ensemble of hypothetical source zones with nonuniform DNAPL distributions dominated by high saturations [*Parker and Park*, 2004; *Park and Parker*, 2005]. The latter distributions, developed using a novel percolation theory-based infiltration model, resulted in relatively high entrapped organic phase saturations (i.e., contaminated cell average $s_n = 0.158$; GTP < 1.0) in the upper (U) regions of the domain and extensive pooling above the lower (L) impermeable boundary (contaminated cell average $s_n = 0.233$; GTP $\ll 1.0$), which, when combined to form a single NAPL distribution (M) resulted in a relatively low GTP [*Parker and Park*, 2004; *Park and Parker*, 2005]. While consideration of these scenarios is important, field conditions will likely fall somewhere between the ganglia-dominated distribution of *Zhu and Sykes* [2004] and the mixed pool-dominated source zone distribution of *Parker and Park* [2004] [e.g., *Poulsen and Kueper*, 1992; *Kueper et al.*, 1993; *Broholm et al.*, 1999].

[12] DNAPL source zones employed in this work are composed of an ensemble of 16 3-D DNAPL saturation distributions selected from a recent modeling study that simulated hysteretic infiltration and entrapment of an immiscible tetrachloroethene (PCE)-NAPL in nonuniform permeability fields using the University of Texas Chemical Flooding Simulator (UTCHEM 9.0) [*Center for Petroleum and Geosystems Engineering*, 2000] (see *Christ et al.* [2005] for simulation details). Hydrogeologic properties were based on data obtained from a contaminated aquifer in Oscoda, Michigan (Bachman Road site), composed of relatively homogeneous glacial outwash sands [*Lemke et al.*, 2004a]. Spill characteristics were selected to be consistent with a slow, sustained release of contaminant. Simulation parameters are summarized in Table 1. Shown in Figure 1a is an example of an initial DNAPL saturation distribution. Here, the simulation domain has been sliced through the center cross section along the direction of flow to show the PCE-NAPL saturations in a representative *x-y* plane. This simulated PCE-NAPL distribution is consistent with

Table 1. Numerical Simulation Input Parameters

Parameter	Water	PCE
Fluid Properties		
Density ρ_α,[a] g cm^{-3}	0.999	1.625
Dynamic viscosity,[a] cP	1.121	0.89
Compressibility,[a] Pa^{-1}	4.4×10^{-10}	0.0
Aqueous diffusivity,[b] cm^2 s^{-1}	-	8.6×10^{-6}
Aqueous solubility,[c] g L^{-1}	-	0.150
Initial saturation	1.0	0.0
Spill Scenario		
Spill volume, L	128	
Spill duration, days	400	
Release rate, L m^{-2} d^{-1}	0.1725	
P_c-s_α-$k_{r\alpha}$ Model Parameters[a]		
Reference air entry pressure, kPa	2.809	
Pore size index	2.0773	
Interfacial tension		
Air/water, dyn cm^{-1}	72.75	
PCE/water, dyn cm^{-1}	47.8	
Irreducible water saturation	0.080	
Max residual organic saturation, s_{nr}^{max}	0.151	
Reference permeability, μm^2	19.7	

Variogram Parameters	Horizontal	Vertical
Matrix Properties[a]		
Nugget	0.333	0.333
Range, m	7.0	1.07
Integral scale, m	2.33	0.36
Mean hydraulic conductivity $\overline{K}$,[a] m d^{-1}	16.8	
Anisotropy ratio k_v/k_h	0.5	
Lognormal transformed $\overline{K}$ variance,[a] $\sigma^2\ln(K)$	0.29	
Applied hydraulic gradient, m m^{-1}	0.01	
Longitudinal dispersivity ω_L,[a] m	0.30	
Horizontal transverse dispersivity ω_{HT},[d] m	0.10	
Vertical transverse dispersivity ω_{HV},[d] m	0.0075	
Median grain size d$_{50}$,[a] μm	295	
Uniformity index U_i[a]	1.86	
Uniform porosity ϕ[a]	0.36	
Δx (m) ($N_x = 26$)	0.3048	
Δy (m) ($N_y = 26$)	0.3048	
Δz (m) ($N_z = 128$)	0.0726	

[a]*Lemke et al.* [2004a].
[b]*Dekker and Abriola* [2000b].
[c]*Horvath* [1982].
[d]*USEPA* [1986].

those generated in previous modeling studies [e.g., *Kueper and Gerhard*, 1995; *Dekker and Abriola*, 2000a; *Lemke et al.*, 2004a] and observed in the field [e.g., *Poulsen and Kueper*, 1992; *Kueper et al.*, 1993; *Broholm et al.*, 1999]. In contrast to the scenarios used by *Zhu and Sykes* [2004] and *Park and Parker* [2005], the DNAPL spill scenarios simulated herein resulted in a mixture of low-saturation ganglia ($0.0001 < s_n < 0.15$) and high-saturation pooled ($0.15 \leq s_n < 0.7$) regions, without accumulation of DNAPL above the lower impermeable boundary. Hence the ensemble of saturation distributions used herein is distributed between two end-members represented by the existing upscaled modeling studies of *Zhu and Sykes* [2004] and *Parker and Park* [2004], and provides realistic scenarios along the continuum of potential DNAPL source zone architectures.

[13] To simulate DNAPL dissolution and mass recovery from the selected saturation distribution scenarios, the component mass balance equation was solved using an existing three-dimensional (3-D), multiphase compositional simula-

tor; the modular three-dimensional transport simulator (MT3D) [*Zheng and Wang*, 1999], modified by *Parker and Park* [2004]. Changes in bulk aqueous phase flow due to DNAPL dissolution were computed using MODFLOW (VERSION 1.10) [*McDonald and Harbaugh*, 1988], modified to update aqueous phase mobility at each time step [*Parker and Park*, 2004]. Interphase mass transfer between the aqueous and solid phases (i.e., sorption) was assumed to be negligible. Mass transfer between the organic liquid and aqueous phases was modeled using (2), with $\kappa_{\alpha\beta i}$ obtained from the *Powers et al.* [1994] correlation:

$$N_{Sh} = 4.13(N_{Re})^{0.598}\left(\frac{d_{50}}{d_M}\right)^{0.673} U_i^{0.369}\left(\frac{s_n}{s_n^o}\right)^{\left(0.518+0.114\left(\frac{d_{50}}{d_M}\right)+0.10U_i\right)}$$

(4)

where d_M is the diameter of a "medium-sized" sand grain ($d_M = 0.05$ cm) according to the ASTM particle size classi-
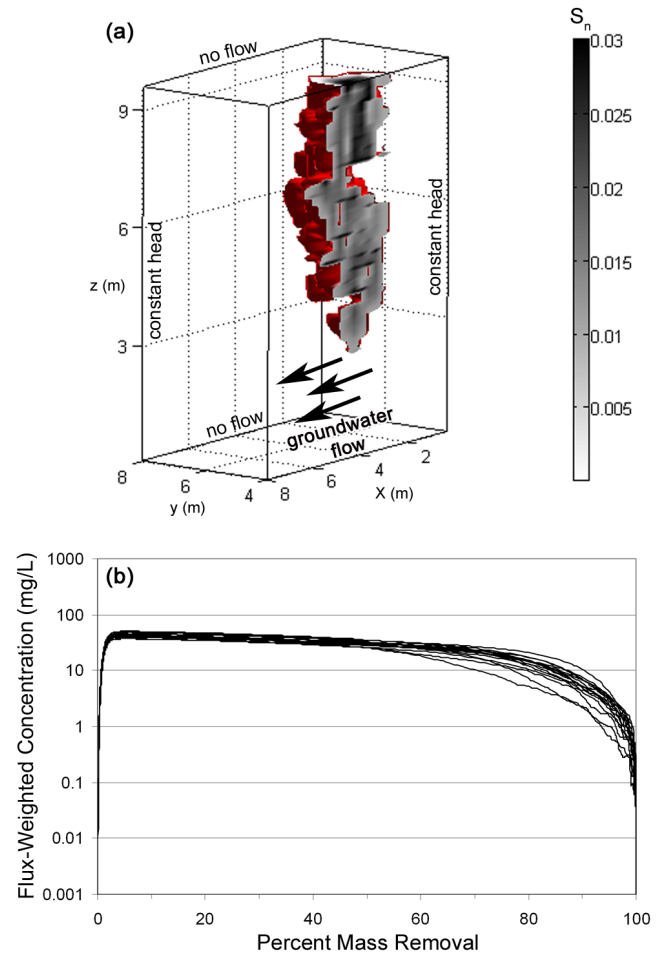

Figure 1. (a) Example of initial DNAPL saturation distribution (GTP = 23.0) sliced through center cross section to illustrate nonuniform DNAPL saturations in x-y plane and (b) flux-weighted PCE concentration curves (light gray lines) across the down-gradient boundary for ensemble of 16 numerical simulations. Note that the red surface represents the $s_n = 0.0001$ isosurface and that the range of s_n was selected to differentiate nonuniformities in low s_n values. Cells with $s_n > 0.03$ are shaded black.

fication, U_i is the uniformity index (d_{60}/d_{10}), s_n^o is the DNAPL saturation at time $t = 0$, and all other parameters are as defined previously. The modified version of MT3D was used to simulate mass recovery until 99.99% of the DNAPL mass was removed, which resulted in simulated source longevities between 5,000 and ~30,000 days.

[14] Similar correlations have been used extensively in the literature [*Mayer and Miller*, 1996; *Powers et al.*, 1998; *Zhu and Sykes*, 2000; *Brusseau et al.*, 2002] to describe the local (i.e., grid) scale mass transfer coefficient as a function of chemical properties and system parameters. The correlation of *Powers et al.* [1994] was derived using effluent concentration data from residual NAPL entrapped in one-dimensional (1-D) columns. The conditions under which the Powers correlation was developed are similar to those employed in the majority of the domains simulated: $0.0008 < s_n < 0.181$, $0.015 < N_{Re} < 0.23$, and $1.19 < U_i < 3.33$. Less than one percent of the DNAPL-contaminated cells had initial saturations exceeding 0.181. Simulations conducted with alternative correlations suggest that the selection of a mass transfer correlation becomes important only at very late time (>95% removal), when the saturation distribution is typically dominated by persistent DNAPL pools (results not shown). Use of a mass transfer correlation based upon ganglia dissolution in this phase of source evolution (i.e., when pools dominate) results in an over prediction of down-gradient concentrations. While this result may be considered conservative for the prediction of down-gradient concentrations, it may yield an under prediction of source longevity. This is discussed further below (see section 3.4).

2.3. Analytical Simulations

[15] Simplification of the governing equations described in section 2.1 is required to derive solutions amenable to analytical techniques [e.g., *Sale and McWhorter*, 2001; *Zhu and Sykes*, 2004; *Parker and Park*, 2004]. Common simplifying assumptions employed in upscaled mass transfer models include (1) approximation of the transient, nonuniform, 3-D flow field by a steady, uniform, 1-D flow field subject to an equivalent average hydraulic flux ($\overline{q}$), (2) negligible transverse dispersivity (ω_T) and molecular diffusion (D_M), (3) quasi-steady state dissolution kinetics, and (4) mass transfer (dissolution) can be described using an upscaled mass transfer coefficient (κ_{eff}) that is a function of domain-averaged parameters [*Dekker*, 1996; *Parker and Park*, 2004; *Park and Parker*, 2005]. Application of assumptions 1 and 2 requires that the down-gradient control plane is sufficiently large such that all of the contaminant mass eluting from the source zone crosses the down-gradient boundary. In practice, the down-gradient control plane must increase as the distance separating the source zone and control plane increases to account for mixing in directions perpendicular to flow. Assumption 3 is typically justified by noting that the timescale for changes in DNAPL saturations (surrogate for interfacial area) during dissolution is relatively large when compared to the hydraulic residence time of the source zone [*Parker and Park*, 2004].

[16] On the basis of the first assumption (1, uniform 1-D $\overline{q}$), the bulk fluid phase flow equation can be neglected.

Application of assumptions 2–4 simplifies the component mass balance equation (1) to yield

$$\overline{q}\left(\frac{d\overline{C}(x)}{dx} - \omega_L \frac{d^2\overline{C}(x)}{dx^2}\right) = \kappa_{eff}\left(C^{eq} - \overline{C}(x)\right) \qquad (5)$$

where $\overline{C}(x)$ is the flux-weighted aqueous phase concentration of a selected component at a distance x from the source, where x is typically assumed to correspond to the down-gradient boundary ($x = L$) of the 1-D domain, ω_L is the longitudinal dispersivity, and C^{eq} is the equilibrium aqueous solubility of the selected component. Equation (5) is a second-order ordinary differential equation that is readily solved by enforcing a type I upstream boundary condition ($\overline{C}(0) = 0$), a type II boundary condition ($d\overline{C}(L)/dx = 0$) at $x = N_x\Delta x = L$, and an initial condition ($\overline{C}(x) = 0$) [*Parker and Park*, 2004]:

$$\frac{\overline{C}(L)}{C^{eq}} = 1 - \exp\left(\frac{L}{2\phi\omega_L}\left(1 - \left(1 + \frac{4\kappa_{eff}\phi\omega_L}{\overline{q}}\right)^{1/2}\right)\right) \qquad (6a)$$

which is readily simplified to

$$\frac{\overline{C}(L)}{C^{eq}} = 1 - \exp\left(\frac{-\kappa_{eff}L}{\overline{q}}\right) \qquad (6b)$$

for $\omega_L/L < 0.1$. The restriction on ω_L/L is reasonable, given that values of longitudinal dispersivity (ω_L) are relatively small when compared to typical distances separating a source zone from the selected down gradient boundary (L) (e.g., $\omega_L = 0.1$ m and $L = 10$ m).

[17] Application of (6a) and (6b) requires that the upscaled mass transfer coefficient (κ_{eff}) be quantified. Previous studies suggest κ_{eff} may be evaluated by assuming that it conforms to a field-scale mass transfer correlation analogous to those presented for local-scale models (e.g., (4)). Best fit mass transfer correlation parameters have been obtained by fitting (6a) and (6b) to numerically generated flux-weighted concentration curves using nonlinear least squares regression [e.g., *Parker and Park*, 2004]. This fitting process yields a system-optimized, upscaled mass transfer correlation, which approximates the dissolution behavior of a particular (but unknown) nonuniform distribution of DNAPL within the source zone. Application of (6a) and (6b) with the best fit upscaled mass transfer correlation is motivated by the prospect of predicting source zone mass discharge at other sites with unknown DNAPL saturation distributions, but similar source zone characteristics [e.g., *Parker and Park*, 2004; *Falta et al.*, 2005a; *Park and Parker*, 2005].

[18] Source longevity predictions may also be made using an upscaled mass transfer model by enforcing a mass balance condition:

$$\frac{dM}{dt} = -\overline{q}A_b\overline{C}(L) \qquad (7)$$

Here the reduction in the amount of DNAPL mass within the source zone is related to the amount of mass exiting the

Table 2. Summary of Simplified Upscaled Mass Transfer Models

Reference	Assumptions	Regression Equation	κ_{eff} Correlation
Dekker [1996]	1, 2[a]	$\phi s_a \frac{\partial \overline{C}}{\partial t} - \frac{\partial}{\partial x}\left(\phi s_a D_i^{h^a}\frac{\partial \overline{C}}{\partial x}\right) + \overline{q}\frac{\partial \overline{C}}{\partial x} = \kappa_{eff}\left(C^{eq} - \overline{C}\right)$ solved using finite element method	$\kappa_o \frac{z_{pen}}{N_z \Delta z}\left(\frac{s_a^{avg}}{s_a^{avg}(t=0)}\right)^{\beta}$
Parker and Park [2004]	1, 2, 3, 4[a]	$\frac{\overline{C}(L)}{C^{eq}} = 1 - \exp\left(\frac{-\kappa_{eff}L}{\overline{q}}\right)$ note $\frac{\overline{C}(L)}{C^{eq}} \approx \frac{\kappa_{eff}L}{\overline{q}}$ for $\kappa_{eff}L/\overline{q} \ll 1$	$\kappa_o\left(\frac{\overline{q}}{\overline{K}}\right)^{\gamma}\left(\frac{M(t)}{M(t=0)}\right)^{\beta}$ $\gamma = 1$ in all simulations
Zhu and Sykes [2004][b]	$\overline{C}\alpha M(t)$	L: $\frac{\overline{C}(L)}{C^{eq}} = \frac{M(t)}{M(t=0)}$ NL1: $\frac{\overline{C}(L)}{C^{eq}} = \left(\frac{M(t)}{M(t=0)}\right)^{\beta}$ NL2: $\frac{\overline{C}(L)}{C^{eq}} = \kappa_o\left(\frac{M(t)}{M(t=0)}\right)^{\beta}$	κ_{eff} not specified in this model
Falta et al. [2005a][c]	$\overline{C}\alpha M(t)$	$\frac{\overline{C}(L)}{C_o} = \left(\frac{M(t)}{M(t=0)}\right)^{\beta}$	κ_{eff} not specified in this model

[a]Assumption described in text.
[b]*Zhu and Sykes* [2004] present three simplified models: L, linear model; NL1, nonlinear model 1; and NL2, nonlinear model 2.
[c]C_o reflects the flow-averaged contaminant concentration at the source zone control plane.

domain through the down gradient boundary (A_b) in (7). Substitution of expressions for $\overline{C}(L)$ derived from the upscaled models into (7) provides a simple method for computing the time required to achieve a specified mass reduction based on remediation objectives.

3. Results
3.1. Baseline Numerical Simulations

[19] As described in section 2.2, an ensemble of 16 numerical simulations of mass discharge from a nonuniform PCE source zone were developed and used as a baseline for comparison with predictions obtained from four existing upscaled mass transfer models [*Parker and Park*, 2004; *Zhu and Sykes*, 2004]. Flux-weighted aqueous phase concentrations across the down-gradient domain boundary for all 16 realizations are plotted in Figure 1b. The assumption that PCE-NAPL infiltration occurs in the absence of dissolution results in an initial flux-weighted concentration across the down-gradient domain boundary equal to zero. This flux-weighted concentration rises sharply at very low percent mass removal as dissolution and transport of contaminant begins. Down-gradient concentrations reach ''pseudo-steady state'' values ($\sim$40 mg L^{-1}) after approximately 5% mass removal. Although saturation distributions change due to DNAPL dissolution, the resulting change in flux-weighted concentrations is relatively small until the source zone begins to transition from a ganglia-dominated to a pool-dominated DNAPL distribution. This transition region occurs between 75 and 95% mass removal (1,000–2,000 days) in these simulations, and results in a rapid reduction of contaminant concentration. Concentrations approach zero only after the vast majority (>95%) of the contaminant mass has been removed from the persistent high saturation pools.

3.2. Upscaled Model Assessment

[20] The general method used in upscaled mass transfer modeling (section 2.3) has been employed in the literature along with various simplifying assumptions to derive several upscaled mass transfer models for specific source zone scenarios. These models are summarized in Table 2. Inspection of Table 2 shows that the existing upscaled models range in complexity from a nonsteady, numerically based model [*Dekker*, 1996] to highly simplified models derived

assuming a basic relationship between the flux-weighted effluent concentration and mass depletion [*Zhu and Sykes*, 2004; *Falta et al.*, 2005a]. Regardless of model complexity, however, all upscaled mass transfer correlations employ the same functional form:

$$\kappa_{eff} = \kappa_o'\left(\frac{M(t)}{M_o}\right)^{\beta} \quad (8)$$

where κ_o' and β are fitting parameters and M_o is the DNAPL mass at $t = 0$. Here, κ_o' is a function of system parameters ($\overline{q}$ and L) and is used to account for mixing and dilution as water flows through the nonuniform DNAPL saturation distribution (i.e., mass discharge). *Park and Parker* [2005] recently presented a methodology for computing κ_o' based on aquifer and source zone properties. In contrast, β is a fit parameter used as a surrogate for the saturation architecture that controls the effective rate at which mass transfer occurs during depletion of DNAPL mass.

[21] Sensitivity of these two parameters to source zone conditions can be explored by comparing values derived for different source zone scenarios (see Table 3). To develop row 1 of Table 3, the upscaled model (6a) and (6b) was fit in conjunction with the upscaled mass transfer correlation (8) to each realization of the ensemble of numerically generated mass recovery curves (see Figure 1b). Mean best fit upscaled correlation parameter values and their corresponding 95% confidence intervals are presented in the first row of Table 3. The flux-weighted concentration prediction obtained from the mean of the best fit values in the upscaled mass transfer model is compared to the ensemble of numerical simulations in Figure 2. For comparison purposes, Table 3 also presents mass transfer parameters reported for the correlations presented in Table 2. Recall that the correlations shown in Table 2 were developed from source zone scenarios which differ from those based on the Bachman Road site. Hence these correlations are not expected to result in accurate flux-weighted concentration predictions for the Bachman Road site. Predictions of flux-weighted concentrations shown in Figure 2 illustrate the variability that can be expected when an existing correlation is inappropriately applied to a site

Table 3. Comparison of Best Fit and Published Correlation Parameters for κ_{eff} in Upscaled Mass Transfer Models Shown in Table 2[a]

Reference	System Description	κ'_o, d^{-1}	β
This work (equations (6) and (8))	ensemble of 3-D simulations of nonuniform source zones based on Bachman Road site	8.2×10^{-3} (± 0.06)	0.85 (± 0.07)
Dekker [1996]	2-D simulation of SEAR in nonuniform DNAPL source zones based on Borden (B) and Jussel (J) aquifers[b]	B: 0.14 J, 0.09	B: 0.81 J, 1.5
Parker and Park [2004]	3-D simulation of DNAPL dissolution under natural gradient conditions in upper region (U), lower region (L), and upper and lower region (M) of a single nonuniform DNAPL source zone	U: 4.9×10^{-4} L, 2.4×10^{-5} M, 4.9×10^{-4}	U: 1.10 L, 0.40 M, 1.40
Zhu and Sykes [2004]	1-D column containing a residual saturation of DNAPL using the linear (L), nonlinear 1 (NL1), and nonlinear 2 (NL2) models[c]	L: NA NL1, NA NL2, 0.80	L: NA NL1, 1.10 NL2, 1.31
Falta et al. [2005a]	3-D simulation of NAPL dissolution under natural gradient conditions with organic saturation positively or negatively correlated with permeability	NA	0.5 $-$ 2.0

[a]NA, not applicable.
[b]The Borden and Jussel aquifers differ in their degree of spatial heterogeneity: $\sigma^2 \ln(k) = 0.24$ for Borden and $\sigma^2 \ln(k) = 1.0$ for Jussel [see *Dekker*, 1996; *Dekker and Abriola*, 2000a].
[c]*Zhu and Sykes* [2004] state that this comparison is for illustrative purposes only and was not a true test of the models.

with characteristics that are not consistent with those to which the correlation is calibrated. Note, the *Dekker* [1996] model is excluded from Figure 2 because this model employs numerical methods, which diminishes a key benefit of upscaled modeling approaches; ease of use. The *Falta et al.* [2005a] model has also been excluded from Figure 2 because it is essentially the same model as the *Zhu and Sykes* [2004] NL2 model.

[22] Inspection of the parameter values reported in Table 3 reveals differences among model parameters arise from differences in the source zone conditions used to obtain the best fit correlation parameters. For example, *Parker and Park* [2004] simulated the release of 229 L of trichloroethene (TCE) with a release rate of ~25,000 L m^{-2} d^{-1} from a single cell into a randomly generated permeability field with a mean saturated hydraulic conductivity ($\overline{K}$) of 10 m d^{-1} and a $\ln(K)$ variance ($\sigma^2 \ln(K)$) of 1. This relatively high release rate, combined with a lack of capillary entrapment in the percolation model, led to high TCE saturations (GTP ≈ 0.414 assuming "fingers" and "lenses" values presented in Table 1 of *Parker and Park* [2004] correspond to ganglia and pools, respectively) distributed nonuniformly throughout a relatively small region of the domain (~10% of the 10 $\times$ 10 m footprint) and resulted in dilution of the flux-weighted concentration across the down-gradient boundary ($\overline{C}(L)$). Fitting this diluted, flux-weighted concentration resulted in κ'_o values that are more than an order of magnitude less than the parameters obtained with the other correlations (see Table 3), regardless of which region of the domain was considered (upper (U), lower (L), or mixed (M), see Table 2). As shown in Figure 2 for the conditions considered here, a low κ'_o value translates to a relatively low quasi-steady state contaminant concentration prediction. In contrast, *Zhu and Sykes* [2004] considered a hypothetical 2-D (x-z) domain that contained a fully penetrating (z direction), residually saturated ($s_n = 0.01$) region with a GTP = ∞. This relatively simple source zone scenario leads to higher best fit κ'_o values, which result in near-saturation quasi-steady state contaminant concentration predictions (Figure 2). Variability among the fitted values of β (mass depletion parameter) was within a factor of three. Low values of β (<1.0) generally correspond to saturation

distributions dominated by DNAPL pools. High β values (>1.0) correspond to DNAPL saturation distributions dominated by DNAPL ganglia.

[23] Relative differences between upscaled model predictions of flux-weighted concentrations and the mean flux-weighted concentration of the numerical simulations can be quantified using objective functions such as the root-mean-square error (RMSE). RMSE was computed at 5% mass removal increments starting at the mass removal level corresponding to the establishment of quasi-steady state conditions (i.e., 5%) and ending at 99.99% mass removal. RMSE values for the upscaled models depicted in Figure 2 are listed in Table 4. Use of an upscaled model developed under alternative site conditions to predict flux-weighted concentrations for the conditions of the numerical simulations considered in this work results in either an overprediction (*Zhu and Sykes* [2004] models) or underprediction (*Parker and Park* [2004] M) of the flux-weighted concentration. The upscaled model fit to the ensemble of 16 numerical simulations provides the lowest RMSE. It is important to note, however, that even when the upscaled
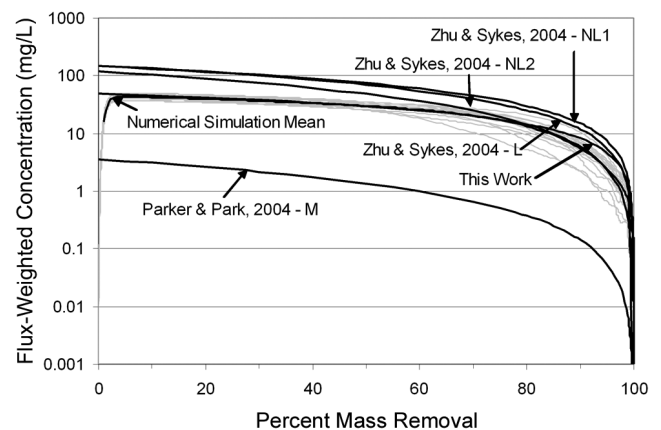

Figure 2. Flux-weighted PCE concentration as a function of mass reduction for 16 numerical simulations (light gray lines) and upscaled mass transfer models listed in Table 2. Model input parameters are given in Tables 1, 2, and 3.

Table 4. Root-Mean-Square Error of Upscaled Models When Compared to the Mean of the Numerical Simulations[a]

Upscaled Model	RMSE, mg L^{-1}
This work (equations (6) and (8))	1.8
Parker and Park [2004] M	27.3
Zhu and Sykes [2004] L	53.0
Zhu and Sykes [2004] NL1	50.1
Zhu and Sykes [2004] NL2	30.6

[a]Note that RMSE computed at mass removal increments of 5% starting at the 5% mass removal level and ending at 99.99% mass removal.

mass transfer parameters are fit to the numerical simulations (this work), flux-weighted concentration predictions can overestimate or underestimate the flux-weighted concentration for any individual realization (light gray lines in Figure 2) by an order of magnitude.

[24] An alternative metric for evaluating the performance of upscaled mass transfer models is source longevity (equation 7). Source longevity predictions using upscaled models are compared to source longevity statistics for the 16 numerical simulations in Table 5. Overestimation of the flux-weighted concentrations [e.g., *Zhu and Sykes*, 2004] resulted in relatively short cleanup times (reduced source longevity), whereas underestimation of flux-weighted concentrations (e.g., *Parker and Park* [2004] M model) resulted in increased source longevity (by up to one order of magnitude). The time required to achieve higher levels of mass removal (e.g., 99.99%) has been shown to depend on the presence or absence of persistent, discontinuous DNAPL pools [*Lemke et al.*, 2004b; *Lemke and Abriola*, 2006]. Given that the mass depletion exponent, β, is derived by fitting the entire DNAPL mass depletion curve, it is unlikely that upscaled mass transfer models can predict flux-weighted concentrations at large times, when DNAPL ganglia have dissolved and discrete DNAPL pools remain. Hence, as the level of mass removal increases from 90% to 99.99%, the disparity between upscaled source longevity predictions and the average source longevity prediction obtained from the numerical simulations will likely grow larger.

3.3. Pseudosteady State Concentration

[25] The analysis presented above indicates that predictions of flux-weighted concentrations and source longevity using upscaled models can substantially deviate from numerical simulation results when the models are applied to sites with NAPL saturation distributions uncharacteristic of those that were used to calibrate the upscaled correlation parameters. Most upscaled model predictions shown in Figure 2 result in higher flux-weighted concentrations than those obtained for the average numerical simulation, which may be considered a conservative estimate with respect to maximum contaminant level (MCL) compliance criteria. However, higher flux-weighted concentration values also result in the underestimation of source longevity or cleanup time (see Table 5). It may therefore be advantageous to modify the upscaled mass transfer correlation (8) to obtain more accurate estimates of the initial flux-weighted contaminant concentrations.

[26] Two possible approaches for improving the predictive capabilities of the upscaled mass transfer correlation are (1) incorporation of additional parameters in the correlation to account for the effects of flow bypassing on the flux-weighted concentrations and (2) modification of an existing parameter in the correlation (e.g., κ_o) to more accurately represent flux-weighted concentrations. *Dekker* [1996] employed the first type of modification by incorporating the depth of the DNAPL saturation distribution (depth of penetration, z_{pen}) normalized by the depth to the lower impermeable boundary ($N_z\Delta z$) into the upscaled mass transfer correlation to account for dilution at the down-gradient boundary (see Table 2). An analogous approach could be used in 3-D to modify the down gradient boundary area to be consistent with the horizontal spread of the saturation distribution, e.g.,

$$\kappa_{eff} = \kappa_o \frac{A_c}{A_b} \left(\frac{M(t)}{M(t=0)} \right)^{\beta} \tag{9}$$

where A_c is the contaminated area of the down gradient boundary area (A_b). Quantification of A_c requires delineation of the extent of the dissolved-phase contaminant plume at a selected concentration (e.g., MCL). Precise delineation of the contaminant concentration profile is a potentially difficult task in the field, particularly for source zones with high degrees of nonuniformity.

[27] Alternatively, inspection of the best fit upscaled simulation shown in Figure 2 indicates that the initial flux-weighted concentration ($t \approx 0$, $M/M_o \approx 1$) is approximately equivalent to the pseudo-steady state flux-weighted concentration predicted using the upscaled model. Assuming that the initial flux-weighted concentration ($\overline{C_o}$) could be obtained from preliminary site characterization data,

Table 5. Source Longevity Predicted Using the Numerical and Upscaled Mass Transfer Models[a]

Numerical Simulation	*Parker and Park* [2004] M	*Zhu and Sykes* [2004]	Upscaled Model (6)	Modified Upscaled Model (14)
		90% Mass Removal		
Minimum 2.2	130.2	L, 0.9	minimum 4.4	minimum 4.4
Mean 4.9		NL1, 1.9	mean 5.7	mean 5.6
Maximum 12.7		NL2, 2.6	maximum 8.8	maximum 7.2
		99.99% Mass Removal		
Minimum 13.9	1279	L, 3.7	minimum 8.3	minimum 7.6
Mean 27.4		NL1, 4.8	mean 20.8	mean 14
Maximum 89.7		NL2, 6.7	maximum 102.2	maximum 29.7

[a]Source longevity is defined here as the time in years to remove 90% or 99.99% of the initial DNAPL mass.
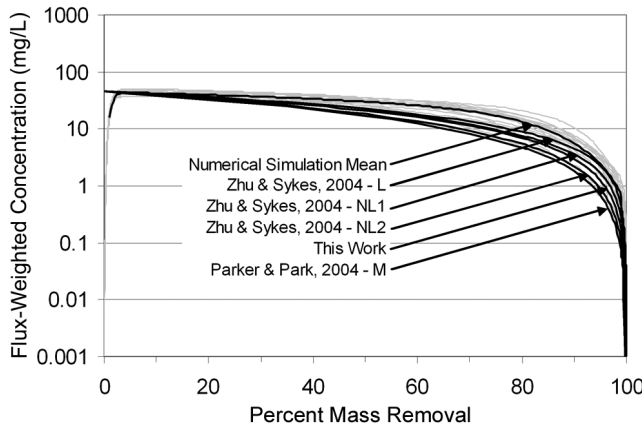
Figure 3. Flux-weighted PCE concentrations as a function of mass reduction for 16 numerical simulations (light gray lines) and upscaled mass transfer models modified as described in the text (equations (11) and (12)). Model parameters are given in Tables 1 and 3.

equations reported in Table 2 may be rearranged to compute, rather than fit, κ'_o. For example, the *Parker and Park* [2004] equation can be rearranged to compute κ_o as a function of system properties and $\overline{C_o}$:

$$\kappa_o = -\frac{\overline{q}}{L} \ln\left(1 - \frac{\overline{C_o}}{C^{eq}}\right) \qquad (10)$$

Flux-weighted concentrations at the down-gradient boundary may then be determined by substituting (10) into the regression equation used to obtain best fit parameters for κ_{eff} ((6a), (6b), and (8)):

$$\frac{\overline{C}(L)}{C^{eq}} = 1 - \left(1 - \frac{\overline{C_o}}{C^{eq}}\right)^{\left(\frac{M}{M_o}\right)^{\beta}} \qquad (11)$$

Only one fitting parameter (β) is included in (11). The best fit parameter, κ'_o, has been replaced with a parameter ($\overline{C_o}$) that may be measured in the field. Performing this same analysis for the other upscaled mass transfer models (*Zhu and Sykes* [2004], *Falta et al.* [2005a], and simplified (i.e., $\kappa_{eff}L/\overline{q} \ll 1$) *Parker and Park* [2004]) yields

$$\frac{\overline{C}(L)}{C^{eq}} = \frac{\overline{C_o}}{C^{eq}}\left(\frac{M}{M_o}\right)^{\beta} \qquad (12)$$

Note that the dependence of equation (12) on the source zone architecture (β), despite the assumption that $\kappa_{eff}L/\overline{q} \ll 1$ (i.e., nonequilibrium), stems from the assumption that κ_{eff} is linearly related to $\overline{q}/L$.

[28] Improvements in the predictions obtained using (11) or (12), depending on the model, are shown in Figure 3. All upscaled mass transfer models now yield pseudo-steady state flux-weighted concentration predictions within 67% of the mean of the numerical simulations. The corresponding RMSE for each of the modified models was reduced by a factor between 3 and 10. These RMSE

values are consistent with the RMSE obtained when fitting the upscaled mass transfer model (equations 6a, 6b and 8) to the numerical simulations, but require only one measured ($\overline{C_o}$) and one best fit (β) parameter.

3.4. Source Zone Architecture

[29] A number of researchers have recognized the need to incorporate site-specific information describing the source zone architecture into upscaled modeling predictions [*Dekker*, 1996; *Parker and Park*, 2004; *Falta et al.*, 2005a]. As shown in the previous analysis, this information is necessary to accurately predict the rate at which DNAPL mass transfer occurs in the source zone and thus may influence the mass depletion parameter (β). In recent numerical modeling studies, *Lemke et al.* [2004b] and *Lemke and Abriola* [2006] showed that the distribution of DNAPL between ganglia and pool regions, defined using the GTP mass ratio (see section 2.2), controlled the flux-weighted concentration emanating from the source zone. It is hypothesized here that the GTP metric is a better predictor of DNAPL mass dissolution characteristics in a source zone than more traditional metrics (e.g., center of mass, average DNAPL saturation).

[30] A relationship between the mass depletion exponent (β) and the initial GTP saturation distribution was developed from an analysis of the 16 numerical simulations used in this study. Flux-weighted concentration curves for each simulation were fit to (11) by setting $\overline{C_o}$ equal to the numerically simulated pseudo-steady state flux-weighted concentration and then fitting β using a nonlinear least squares regression routine. Shown in Figure 4 is a plot of β versus the GTP for each of the numerical simulations. A statistically significant (p value = 0.0039) negative correlation was obtained between β and GTP, which can be expressed through a power law model ($r^2 = 0.6373$) in the following form:

$$\beta = 1.5 \cdot GTP^{-0.26} \text{ for } 1.5 < GTP < 24.0 \qquad (13)$$

Incorporation of (13) into (11) and (12) results in an upscaled mass transfer model capable of simulating both the
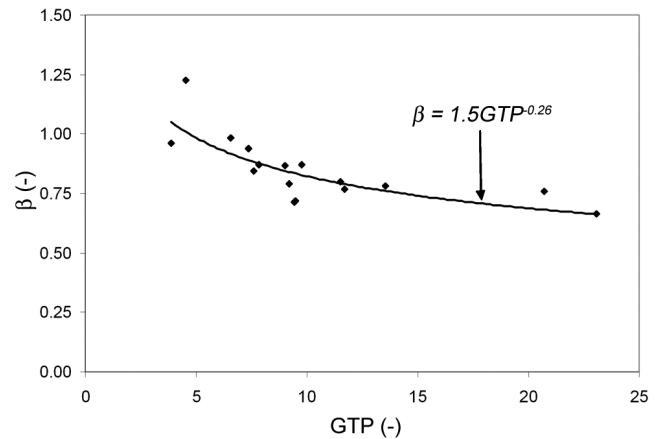

Figure 4. Mass depletion parameter (β) as a function of ganglia-to-pool (GTP) mass ratio for 15 numerical simulations. One simulation with GTP = ∞ was excluded from the figure and correlation.

pseudo-steady state flux-weighted concentration and the transition from ganglia- to pool-dominated dissolution:

$$\frac{\overline{C}(L)}{C^{eq}} = 1 - \left(1 - \frac{\overline{C_o}}{C^{eq}}\right)^{\left(\frac{M}{M_o}\right)^{1.5 \cdot GTP^{-0.26}}} \tag{14a}$$

$$\frac{\overline{C}(L)}{C^{eq}} = \frac{\overline{C_o}}{C^{eq}} \left(\frac{M}{M_o}\right)^{1.5 \cdot GTP^{-0.26}} \tag{14b}$$

Average contaminant concentrations as a function of two site-specific parameters, the initial flux-weighted concentration ($\overline{C_o}$) and the source zone GTP, are included in (14a) and (14b). This formulation does not require fitting to experimental or numerical simulations in order to obtain upscaled correlation parameters. Rather, site-specific field measurements (i.e., $\overline{C_o}$ and GTP) are incorporated directly into the upscaled model, providing a more versatile method for the prediction of the flux-weighted concentration corresponding to a given level of mass removal (M/M_o).

[31] Comparing the proposed upscaled model (14a) prediction of flux-weighted concentration to the mean of the numerical simulations resulted in a RMSE of approximately 2 mg L^{-1}. This RMSE is almost identical to the RMSE for the original upscaled mass transfer model (1.8 mg L^{-1}, Table 4). The mean source longevity value for the proposed (14a) and original (6a) and (6b) upscaled mass transfer models is nearly identical at 90% mass removal (<2% difference), and within 50% at 99.99% mass removal (Table 5). These comparisons demonstrate the ability of the proposed upscaled model to reproduce the predicted values obtained using the original best fit upscaled model without the need to fit scenario-specific correlation parameters.

[32] To examine the ability of the model to be used in a predictive sense, however, the proposed model (14a) and (14b) must be applied to source zone scenarios other than those used to develop the correlation (13). For this evaluation, an ensemble (10 realizations) of published source zone scenarios was selected. Eight of the source zone realizations were selected from a recent numerical modeling study that investigated the relationship between mass discharge and source zone architecture [*Lemke and Abriola*, 2006]. These realizations were developed using sequential indicator simulation (SIS) and assuming there was no correlation between soil (i.e., permeability) and capillary properties (i.e., entry pressure). Source zone saturation distributions generated using SIS were characterized by high saturations and extensive lateral pooling. GTP mass ratios ranged from 0.9 to 65 and mass recovery was simulated assuming a surfactant enhanced aquifer remediation scenario. The remaining two realizations correspond to the simulations used by *Zhu and Sykes* [2004] and *Parker and Park* [2004], which have GTP mass ratios of infinity and $\sim$0.41, respectively. Source zones with GTP values outside the range used in the development of the correlation were selected to show the limitations of the model at low or high GTP values. Flux-weighted concentration predictions made using the proposed

upscaled model (solid line) are compared to the numerical simulation results (open symbol) in Figure 5. GTP mass ratios and RMSE for each source zone simulation are also reported in Figure 5. Initial flux-weighted concentrations ($\overline{C_o}$) were assumed to correspond to the first numerically simulated concentration value. For the simulations of *Lemke and Abriola* [2006] this value did not necessarily correspond to a 0% mass removal level, but was assumed to be a reasonable approximation to the initial flux-weighted concentration value.

[33] Analysis of Figure 5 demonstrates that the proposed upscaled model predicts flux-weighted concentrations with RMSE values that range from 3 to 20 mg L^{-1}. These RMSE's are generally three to five times less than the RMSE values obtained when the previously published models were used for prediction (Table 4). The upscaled model captured the initial pseudo-steady state flux-weighted concentration and generally captured the transition from a ganglia-dominated to a pool-dominated source zone, but in some cases failed to accurately predict the flux-weighted concentration eluting from the source zone at high levels (>80%) of mass removal (e.g., Figure 5c). As discussed previously, this limitation stems from the assumption that the mass depletion exponent is a constant and that the correlation is based upon scenarios characterized by relatively high GTP mass ratios. Substituting (13), which is a function of the initial GTP mass ratio, for this mass depletion exponent improves the ability of the upscaled model to simulate the transition from a ganglia- to a pool-dominated source zone, however, it does not account for the eventual transition to a source zone dominated by discreet DNAPL pools. The observation that this discrepancy generally occurs for source zones with low initial GTP mass ratios (Figures 5a−5c) is a further indication of the importance of DNAPL pools in determining the contaminant flux eluting from a nonuniform source zone.

[34] A second limitation of this model is the need to estimate the initial DNAPL source zone GTP mass ratio. Currently, there is a lack of methods to accurately quantify DNAPL saturation distributions in the field. Although partitioning interwell tracer tests (PITT) have been used to estimate average NAPL saturations in source zones over the integrated path length [e.g., *Annable et al.*, 1998; *Ramsburg et al.*, 2005], the results are spatially averaged (e.g., 1 m) and thus do not provide the resolution required to distinguish between ganglia-dominated and pool-dominated regions. Resolution in NAPL saturation estimates resulting from PITTs may be increased by locating multiple observation points along a flow path [*Jin et al.*, 1995; *Annable et al.*, 1998; *Rao et al.*, 2000]. *Fure et al.* [2006] suggest that higher-order temporal moments employed for the interpretation of PITT data [*Jawitz et al.*, 2003] may hold promise for identifying source zone metrics which link mass discharge to NAPL architecture. In addition, it may be possible to obtain higher resolution estimates of the spatial distribution of DNAPL mass through the use of geophysical techniques, which have been used to directly estimate in situ DNAPL saturations [e.g., *Chambers et al.*, 2004]. The analysis presented herein clearly demonstrates the importance of incorporation of site-specific parameters into upscaled mass transfer
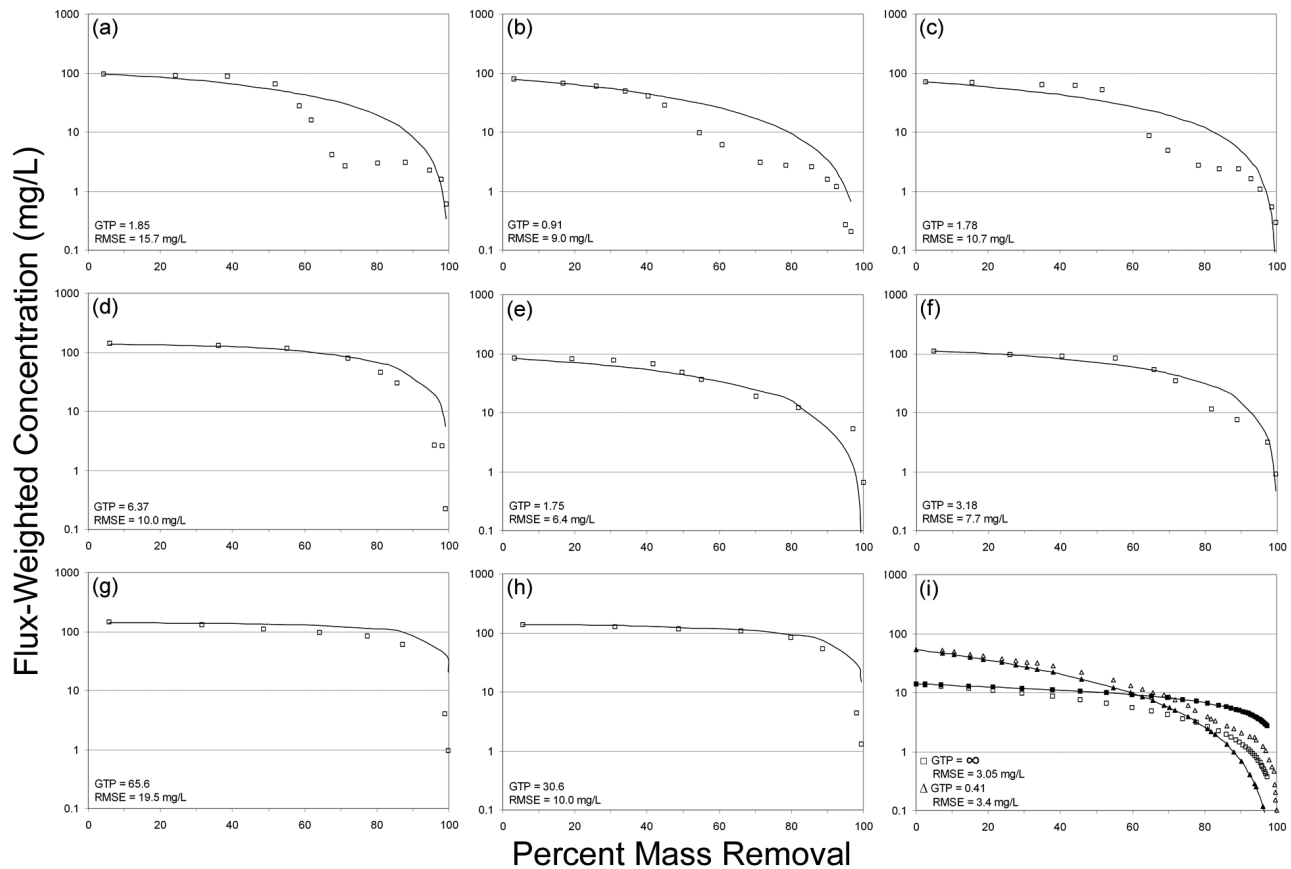
Figure 5. Comparisons of numerical simulation (open symbols) and proposed upscaled mass transfer model (14a) predictions (solid lines) of flux-weighted PCE concentrations as a function of mass removal for realizations selected from *Lemke and Abriola* [2006] (Figures 5a–5h) and *Zhu and Sykes* [2004] (Figure 5i) source zone scenario (GTP = ∞), and *Parker and Park* [2004] source zone scenario (GTP = 0.414). GTP mass ratios and RMSE are (a) 1.85 and 15.7 mg L^{-1}, (b) 0.91 and 9.0 mg L^{-1}, (c) 1.78 and 10.7 mg L^{-1}, (d) 6.37 and 10.0 mg L^{-1}, (e) 1.75 and 6.4 mg L^{-1}, (f) 3.18 and 7.7 mg L^{-1}, (g) 65.6 and 19.5 mg L^{-1}, (h) 30.6 and 10.0 mg L^{-1}, and (i) ∞ and 3.05 mg L^{-1} for *Zhu and Sykes* [2004] and 0.41 and 3.4 mg L^{-1} for *Parker and Park* [2004], respectively.

models and highlights the need for innovations in in situ characterization techniques as an important area for future research.

4. Summary and Conclusions

[35] There is a growing need to develop relatively simple modeling tools to aid site managers and regulators in the monitoring and treatment of DNAPL contaminated source zones. Site-specific numerical simulations are among the most effective methods for evaluating alternative management strategies; however, such models require detailed knowledge of subsurface properties and contaminant distributions. Simplified screening models that utilize upscaled mass transfer coefficients provide an alternative method for simulating average contaminant behavior with less site-specific information and computational cost. The purpose of this work was to evaluate and compare the performance of such upscaled models in capturing average concentrations and source longevity behavior for irregular source zones, and to suggest improvements that allow for a more general prediction capability.

[36] Results from this work demonstrate that many of the existing simplified mass transfer models [*Dekker*, 1996; *Parker and Park*, 2004; *Park and Parker*, 2005; *Zhu and Sykes*, 2004; *Falta et al.*, 2005a] are closely related, with the main differences among these models arising from parameterization of the upscaled mass transfer correlation. Comparisons of predictions obtained using the upscaled models and numerical simulators show that upscaled models may be applied confidently only for the specific conditions under which the correlation parameters were developed, and can either overpredict or underpredict flux-weighted concentrations and source longevities by more than one order of magnitude when applied to other scenarios. This behavior was primarily attributed to the effects of flow bypassing and site-specific saturation distributions on DNAPL dissolution and mass recovery.

[37] To address these limitations, existing upscaled models were modified to replace the fitted upscaled correlation parameters with measurable site-specific parameters. Incorporation of the initial average concentration and ganglia-to-pool mass ratio into the upscaled mass transfer correlation was shown to provide predictions that were similar (within

20%) to those of the best fit model, while maintaining the ability to reasonably predict (RMSE < 10 mg L^{-1}) flux-weighted concentrations eluting from a broad range of source zone scenarios. Limitations of the developed model include the overprediction of flux-weighted concentrations at high levels of mass removal for source zone scenarios that are initially dominated by DNAPL pools, and the need to quantify the initial DNAPL source zone GTP mass ratio. Overprediction of flux-weighted concentrations at high levels of mass removal may lead to underprediction of source longevity. Hence, despite the model's ability to accurately predict flux-weighted concentrations at most levels of mass removal (<85% mass removal), application of the model to predict posttreatment source longevities, particularly at sites with significant DNAPL pooling, should be done with caution.

[38] Future improvement of the predictive capability of upscaled mass transfer models will likely require incorporation of additional site-specific information into the upscaled mass transfer correlation or modification of the upscaled mass transfer model to account for multiple domains possessing different mass transfer characteristics.

References

Abriola, L. M. (1989), Modeling multiphase migration of organic chemicals in groundwater systems—A review and assessment, *Environ. Health Perspect.*, *83*, 117–143.

Abriola, L. M., C. D. Drummond, E. J. Hahn, T. C. G. Kibbey, L. D. Lemke, K. D. Pennell, E. A. Petrovskis, C. A. Ramsburg, and K. M. Rathfelder (2005), A pilot-scale demonstration of surfactant-enhanced PCE solubilization at the Bachman road site: (1) Site characterization and test design, *Environ. Sci. Technol.*, *39*, 1178–1790.

Adeel, Z., J. W. Mercer, and C. R. Faust (2001), Models for describing multiphase flow and transport of contaminants, in *ASCE Manuals and Reports on Engineering Practice No. 100: Groundwater Contamination by Organic Pollutants*, pp. 1–39, Am. Soc. of Civ. Eng., Reston, Va.

Annable, M. D., P. S. C. Rao, K. Hatfield, W. D. Graham, and C. G. Enfield (1998), Partitioning tracers for measuring residual NAPL: Field-scale test results, *J. Environ. Eng.*, *124*, 498–503.

Basu, N. B., P. S. C. Rao, I. C. Poyer, M. D. Annable, and K. Hatfield (2006), Flux-based assessment at a manufacturing site contaminated with trichloroethylene, *J. Contam. Hydrol.*, *86*, 105–127.

Bear, J. (1972), *Dynamics of Fluids in Porous Media*, Elsevier, New York.

Bear, J. (1979), *Hydraulics of Groundwater*, McGraw-Hill, New York.

Berglund, S. (1997), Aquifer remediation by pumping: A model for stochastic-advective transport with nonaqueous phase liquid dissolution, *Water Resour. Res.*, *33*, 399–405.

Broholm, K., S. Feenstra, and J. A. Cherry (1999), Solvent release into a sandy aquifer. 1. Overview of source distribution and dissolution behavior, *Environ. Sci. Technol.*, *33*, 681–690.

Broholm, K., S. Feenstra, and J. A. Cherry (2005), Solvent release into a sandy aquifer. 2. Estimation of DNAPL mass based on a multiple-component dissolution model, *Environ. Sci. Technol.*, *39*, 317–324.

Brusseau, M. L., Z. Zhang, N. T. Nelson, R. B. Cain, G. R. Tick, and M. Oostrom (2002), Dissolution of nonuniformly distributed immiscible liquid: Intermediate-scale experiments and mathematical modeling, *Environ. Sci. Technol.*, *36*, 1033–1041.

Center for Petroleum and Geosystems Engineering (2000), UTCHEM, Version 9.0 technical documentation, Univ. of Tex. at Austin, Austin.

Chambers, J. E., M. H. Loke, R. D. Ogilvy, and P. I. Meldrum (2004), Noninvasive monitoring of DNAPL migration through a saturated porous

medium using electrical impedance tomography, *J. Contam. Hydrol.*, *68*, 1–22.

Christ, J. A., C. A. Ramsburg, L. M. Abriola, K. D. Pennell, and F. E. Löffler (2003), Coupling aggressive mass removal with microbial reductive dechlorination for remediation of DNAPL source zones—A review and assessment, *Environ. Health Perspect.*, *113*, 465–476.

Christ, J. A., L. D. Lemke, and L. M. Abriola (2005), Comparison of two-dimensional and three-dimensional simulations of dense nonaqueous phase liquids (DNAPLs): Migration and entrapment in a nonuniform permeability field, *Water Resour. Res.*, *41*, W01007, doi:10.1029/2004WR003239.

Chrysikopoulos, C. V., and T-J. Kim (2000), Local mass transfer correlations for nonaqueous phase liquid pool dissolution in saturated porous media, *Transp. Porous Media*, *38*, 167–187.

Dekker, T. J. (1996), An assessment of the effects of field-scale formation heterogeneity on surfactant-enhanced aquifer remediation, Doctoral dissertation, Univ. of Michigan, Ann Arbor.

Dekker, T. J., and L. M. Abriola (2000a), The influence of field-scale heterogeneity on the infiltration and entrapment of dense nonaqueous phase liquids in saturated formation, *J. Contam. Hydrol.*, *42*, 187–218.

Dekker, T. J., and L. M. Abriola (2000b), The influence of field-scale heterogeneity on the surfactant-enhanced remediation of entrapped nonaqueous phase liquids, *J. Contam. Hydrol.*, *42*, 219–251.

Einarson, M. D., and D. M. Mackay (2001), Predicting impacts of ground water contamination, *Environ. Sci. Technol.*, *35*, 67A–73A.

Enfield, G. C., A. L. Wood, F. P. Espinoza, M. C. Brooks, M. Annable, and P. S. C. Rao (2005), Design of aquifer remediation systems: (1) Describing hydraulic structure and NAPL architecture using tracers, *J. Contam. Hydrol.*, *81*, 125–147.

Falta, R. W., P. S. Rao, and N. Basu (2005a), Assessing the impacts of partial mass depletion in DNAPL source zones: I. Analytical modeling of source strength functions and plume response, *J. Contam. Hydrol.*, *78*, 259–280.

Falta, R. W., N. Basu, and P. S. Rao (2005b), Assessing impacts of partial mass depletion in DNAPL source zones: II. Coupling source strength functions to plume evolution, *J. Contam. Hydrol.*, *76*, 281–302.

Fetter, C. W. (1993), *Contaminant Hydrogeology*, Prentice-Hall, Upper Saddle River, N. J.

Frind, E. O., J. W. Molson, M. Schirmer, and N. Guiger (1999), Dissolution and mass transfer of multiple organics under field conditions: The Borden emplaced source, *Water Resour. Res.*, *35*, 683–694.

Fure, A. D., J. J. Jawitz, and M. D. Annable (2006), DNAPL source depletion: Linking architecture and flux response, *J. Contam. Hydrol.*, *85*, 118–140.

Geller, J. T., and J. R. Hunt (1993), Mass transfer from nonaqueous phase organic liquids in water-saturated porous media, *Water Resour. Res.*, *29*, 833–845.

Held, R. J., and M. A. Celia (2001), Pore-scale modeling and upscaling of nonaqueous phase liquid mass transfer, *Water Resour. Res.*, *37*, 539–549.

Horvath, A. L. (1982), *Halogenated Hydrocarbons Solubility: Miscibility With Water*, CRC Press, Boca Raton, Fla.

Imhoff, P. T., P. R. Jaffe, and G. R. Pinder (1994), An experimental study of complete dissolution of a nonaqueous phase liquid in saturated porous media, *Water Resour. Res.*, *30*, 307–320.

Jawitz, J. W., M. D. Annable, G. G. Demmy, and P. S. C. Rao (2003), Estimating nonaqueous phase liquid spatial variability using partitioning tracer higher temporal moments, *Water Resour. Res.*, *39*(7), 1192, doi:10.1029/2002WR001309.

Jawitz, J. T., A. D. Fure, G. G. Demmy, S. Berglund, and P. S. C. Rao (2005), Groundwater contaminant flux reduction resulting from nonaqueous phase liquid mass reduction, *Water Resour. Res.*, *41*, W10408, doi:10.1029/2004WR003825.

Jia, C., K. Shing, and Y. C. Yortsos (1999), Advective mass transfer from stationary sources in porous media, *Water Resour. Res.*, *35*, 3239–3251.

Jin, M., M. Delshad, V. Dwarakanath, D. C. McKinney, G. A. Pope, K. Sepehrnoori, C. E. Tilburg, and R. E. Jackson (1995), Partitioning tracer tests for detection, estimation, and remediation performance assessment of subsurface nonaqueous phase liquids, *Water Resour. Res.*, *31*, 1201–1211.

Kim, T.-J., and C. V. Chrysikopoulos (1999), Mass transfer correlations for nonaqueous phase liquid pool dissolution in saturated porous media, *Water Resour. Res.*, *35*, 449–459.

Kueper, B. H., and J. I. Gerhard (1995), Variability of point source infiltration rates for two-phase flow in heterogeneous porous media, *Water Resour. Res.*, *31*, 2971–2980.

Kueper, B. H., D. Redman, R. C. Star, S. Reitsma, and M. Mah (1993), A field experiment to study the behavior of tetrachloroethylene below the water table: Spatial distribution of residual and pooled DNAPL, *Ground Water*, 31, 756–766.

Lemke, L. D., and L. M. Abriola (2006), Modeling DNAPL mass removal in nonuniform formations: Linking source zone architecture and system response, *Geosphere*, 2, 74–82.

Lemke, L. D., L. M. Abriola, and P. Goovaerts (2004a), DNAPL source zone characterization: Influence of hydraulic property correlation on predictions of DNAPL infiltration and entrapment, *Water Resour. Res.*, 40, W01511, doi:10.1029/2003WR001980.

Lemke, L. D., L. M. Abriola, and J. R. Lang (2004b), DNAPL source zone remediation: Influence of source zone architecture on predictions of DNAPL recovery and contaminant flux, *Water Resour. Res.*, 40, W12417, doi:10.1029/2004WR003061.

Mackay, D. M., and J. A. Cherry (1989), Groundwater contamination: Pump-and-treat remediation, *Environ. Sci. Technol.*, 23, 630–636.

Mayer, A. S., and C. T. Miller (1996), The influence of mass transfer characteristics and porous media heterogeneity on nonaqueous phase dissolution, *Water Resour. Res.*, 32, 1551–1568.

McDonald, M. G., and A. W. Harbaugh (1988), A modular three-dimensional finite difference groundwater flow model, in *Modeling Techniques*, U.S. Geol. Surv. Tech. of Water Resour. Invest., Book 6, Chapter A1, 586 pp.

McWhorter, D. B., and T. C. Sale (2003), Reply to comment by P. S. C. Rao and J. W. Jawitz on "Steady state mass transfer from single-component dense nonaqueous phase liquids in uniform flow fields" by T. C. Sale and D. B. McWhorter, *Water Resour. Res.*, 39(3), 1069, doi:10.1029/2002WR001423.

Mercer, J. W., and R. M. Cohen (1990), A review of immiscible fluids in the subsurface: Properties, models, characterization, and remediation, *J. Contam. Hydrol.*, 6, 107–163.

Miller, C. T., M. M. Poirier-McNeill, and A. S. Mayer (1990), Dissolution of trapped nonaqueous phase liquids: Mass transfer characteristics, *Water Resour. Res.*, 26, 2783–2796.

Miller, C. T., G. Christakos, P. T. Imhoff, J. F. McBride, J. A. Pedit, and J. A. Trangenstein (1998), Multiphase flow and transport modeling in heterogeneous porous media: Challenges and approaches, *Adv. Water Resour.*, 21, 77–120.

Nambi, I. M., and S. E. Powers (2000), NAPL dissolution in heterogeneous systems: An experimental investigation in a simple heterogeneous system, *J. Contam. Hydrol.*, 44, 161–184.

Nambi, I. M., and S. E. Powers (2003), Mass transfer correlations for nonaqueous phase liquid dissolution from regions with high initial saturations, *Water Resour. Res.*, 39(2), 1030, doi:10.1029/2001WR000667.

National Research Council (NRC) (2005), *Contaminants in the Subsurface: Source Zone Assessment and Remediation*, Natl. Acad. Press, Washington, D. C.

Park, E., and J. C. Parker (2005), Evaluation of an upscaled model for DNAPL dissolution kinetics in heterogeneous aquifers, *Adv. Water Resour.*, 28, 1280–1291, doi:10.1016/j.advwatres.2005.04.002.

Parker, J. C., and R. J. Lenhard (1987), A model for hysteretic constitutive relations governing multiphase flow: 1. Saturation-pressure relations, *Water Resour. Res.*, 23, 2187–2196.

Parker, J. C., and E. Park (2004), Modeling field-scale dense nonaqueous phase liquid dissolution kinetics in heterogeneous aquifers, *Water Resour. Res.*, 40, W05109, doi:10.1029/2003WR002807.

Poulsen, M. M., and B. H. Kueper (1992), A field experiment to study the behavior of tetrachloroethylene in unsaturated porous media, *Environ. Sci. Technol.*, 26, 889–895.

Powers, S. E., L. M. Abriola, and W. J. Weber Jr. (1994), An experimental investigation of nonaqueous phase liquid dissolution in saturated subsurface systems: Transient mass transfer rates, *Water Resour. Res.*, 30, 321–332.

Powers, S. E., I. M. Nambi, and G. W. Curry Jr. (1998), Nonaqueous phase liquid dissolution in heterogeneous systems: Mechanisms and a local equilibrium modeling approach, *Water Resour. Res.*, 34, 3293–3302.

Ramsburg, C. A., K. D. Pennell, L. M. Abriola, G. Daniels, C. D. Drummond, M. Gamache, H. Hsu, E. Petroskis, K. M. Rathfelder, J. Ryder, and T. Yavaraski (2005), A pilot-scale demonstration of surfactant-enhanced PCE solubilization at the Bachman Road site: (2) System operation and evaluation, *Environ. Sci. Technol.*, 39, 1791–1801.

Rao, P. S. C., and J. W. Jawitz (2003), Comment on "Steady state mass transfer from single-component dense nonaqueous phase liquids in uni-form flow fields" by T. C. Sale and D. B. McWhorter, *Water Resour. Res.*, 39(3), 1068, doi:10.1029/2001WR000599.

Rao, P. S. C., M. D. Annable, and H. Kim (2000), NAPL source zone characterization and remediation technology performance assessment: Recent developments and applications of tracer techniques, *J. Contam. Hydrol.*, 45, 63–78.

Rao, P. S. C., J. W. Jawitz, G. C. Enfield, R. W. Falta, M. D. Annable, and A. L. Wood (2001), Technology integration for contaminated site remediation: Clean-up goals and performance criteria, in *Groundwater Quality 2001: Natural and Enhanced Restoration of Groundwater Pollution, Proceedings of the 3rd International Conference, Sheffield, England, June 18–21*, edited by S. F. Thornton and S. E. Oswald, IAHS Publ., 273, 410–412.

Rivett, M. O., and S. Feenstra (2004), Dissolution of an emplaced source of DNAPL in a natural aquifer setting, *Environ. Sci. Technol.*, 39, 447–455, doi:10.1021/es040016f.

Saba, T., and T. H. Illangasekare (2000), Effect of groundwater flow dimensionality on mass transfer from entrapped nonaqueous phase liquid contaminants, *Water Resour. Res.*, 36, 971–979.

Saenton, S., T. H. Illangasekare, K. Soga, and T. A. Saba (2002), Effects of source zone heterogeneity on surfactant-enhanced NAPL dissolution and resulting remediation end-points, *J. Contam. Hydrol.*, 59, 27–44.

Sale, T. C., and D. B. McWhorter (2001), Steady state mass transfer from single-component dense nonaqueous phase liquids in uniform flow fields, *Water Resour. Res.*, 37, 393–404.

Schaerlaekens, J., and J. Feyen (2004), Effect of scale and dimensionality on the surfactant-enhanced solubilization of a residual DNAPL contamination, *J. Contam. Hydrol.*, 71, 283–306.

Soga, K., J. W. E. Page, and T. H. Illangasekare (2004), A review of NAPL source zone remediation efficiency and the mass flux approach, *J. Hazard. Mater.*, 110, 13–27.

Stroo, H. F., M. Unger, C. H. Ward, M. C. Kavanaugh, C. Vogel, A. Leeson, J. A. Marquesee, and B. P. Smith (2003), Remediating chlorinated solvent source zones, *Environ. Sci. Technol.*, 37, 224A–230A.

U.S. Environmental Protection Agency (USEPA) (1986), Background document for the ground-water screening procedure to support 40 CFR Part 269: Land disposal, *Rep. EPA/530-SW-86-047*, Washington, D. C.

U.S. Environmental Protection Agency (USEPA) (1990), Laboratory investigation of residual liquid organics from spills, leaks, and disposal of hazardous wastes in groundwater, *Rep. EPA/600/6-90/004*, Washington, D. C.

U.S. Environmental Protection Agency (USEPA) (2003), The DNAPL remediation challenge: Is there a case for source depletion?, *Rep. EPA/600/R-03-143*, Washington, D. C.

Weber, W. J., Jr., and F. A. DiGiano (1996), *Process Dynamics in Environmental Systems*, John Wiley, Hoboken, N. J.

Wood, A. L., C. G. Enfield, F. P. Espinoza, M. Annable, M. C. Brooks, P. S. C. Rao, D. Sabatini, and R. Knox (2005), Design of Aquifer remediation systems: (2) Estimating site-specific performance and benefits of partial source removal, *J. Contam. Hydrol.*, 81, 148–166.

Zheng, C., and P. P. Wang (1999), MT3DMS: A modular three-dimensional multispecies transport model for simulation of advection, dispersion, and chemical reactions of contaminants in groundwater systems: Documentation and user's guide, contract report SERDP-99-1, U.S. Army Eng. Res. and Dev. Center, Vicksburg, Miss.

Zhu, J., and J. F. Sykes (2000), The influence of NAPL dissolution characteristics on field-scale contaminant transport in subsurface, *J. Contam. Hydrol.*, 41, 133–154.

Zhu, J., and J. F. Sykes (2004), Simple screening models of NAPL dissolution in the subsurface, *J. Contam. Hydrol.*, 72, 245–258.

————————————

L. M. Abriola and C. A. Ramsburg, Department of Civil and Environmental Engineering, Tufts University, 113 Anderson Hall, 200 College Avenue, Medford MA 02155, USA. (linda.abriola@tufts.edu)

J. A. Christ, Department of Civil and Environmental Engineering, U.S. Air Force Academy, 2343 Fairchild Drive, Suite 6J-159, USAF Academy, CO 80840-6236, USA. (john.christ@usafa.af.mil)

K. D. Pennell, School of Civil and Environmental Engineering, Georgia Institute of Technology, 311 Ferst Drive, Atlanta, GA 30332-0512, USA.